Bayesian assessment of uncertainty in aerosol size distributions and index of refraction retrieved from multiwavelength lidar measurements

Benjamin R. Herman, Barry Gross, Fred Moshary, and Samir Ahmed

Department of Electrical Engineering, Optical Remote Sensing Laboratory City College of the City University of New York, Convent Avenue at 140th Street, New York, New York 10031, USA

*Corresponding author: gross@ccny.cuny.edu

Received 26 September 2007; accepted 27 November 2007;
posted 24 January 2008 (Doc. ID 87966); published 31 March 2008

We investigate the assessment of uncertainty in the inference of aerosol size distributions from backscatter and extinction measurements that can be obtained from a modern elastic/Raman lidar system with a Nd:YAG laser transmitter. To calculate the uncertainty, an analytic formula for the correlated probability density function (PDF) describing the error for an optical coefficient ratio is derived based on a normally distributed fractional error in the optical coefficients. Assuming a monomodal lognormal particle size distribution of spherical, homogeneous particles with a known index of refraction, we compare the assessment of uncertainty using a more conventional forward Monte Carlo method with that obtained from a Bayesian posterior PDF assuming a uniform prior PDF and show that substantial differences between the two methods exist. In addition, we use the posterior PDF formalism, which was extended to include an unknown refractive index, to find credible sets for a variety of optical measurement scenarios. We find the uncertainty is greatly reduced with the addition of suitable extinction measurements in contrast to the inclusion of extra backscatter coefficients, which we show to have a minimal effect and strengthens similar observations based on numerical regularization methods.

OCIS codes: 000.5490, 280.1100, 280.3640.

1. Introduction

Aerosol microphysical parameters including particle size distribution parameters and refractive index are crucial for an understanding of climate effects [1,2]. While most efforts have been oriented toward passive sensors utilizing multispectral scattering and/or extinction [3–8], the recent deployment of multiwavelength elastic and Raman lidars [9,10], which can be processed to obtain multiwavelength measurements of extinction and backscatter coefficients offer the possibility of retrieving the vertical structure of microphysical properties. Unfortunately, even if continuous backscatter and extinction spectra can be obtained, the inversion of the optical coefficient spectra to obtain microphysical parameters is mathematically ill-posed. This problem is magnified further by the limited number of wavelength channels. For example, even the most sophisticated of systems can measure only six backscatter and two extinction coefficients [11].

To further complicate the problem, aerosol optical coefficients retrieved with lidar can have substantial errors due to the deviation between assumed and true molecular atmospheric components, an imperfect knowledge of the range dependent geometric form factor, an incorrect assumption of the aerosol extinction–backscatter ratio and its range dependence in elastic-only lidar systems, multiple scattering, etc. For these reasons, a meaningful estimation of aerosol properties from lidar measurements

0003-6935/08/101617-11$15.00/0

requires a robust assessment of uncertainty, which does not depend on the manner of performing the assessment.

In connecting the optical coefficients to the microphysical aerosol parameters, the basic equations that relate backscatter and extinction coefficients to an aerosol size distribution have the general form

$$y_i = \int_0^\infty K_i(r) n(r) \mathrm{d}r, \tag{1}$$

with y_i representing either the extinction or backscatter coefficients at the ith wavelength, the kernels $K_i(r)$ representing the backscatter or extinction cross section of a single particle with radius r, and $n(r)$ representing the particle size distribution function. In this paper we assume that the particles are spherical, and therefore the kernels take the form $K_i(r) = Q_{[\mathrm{ext}][\mathrm{back}]}(2\pi r/\lambda_i, m)\pi r^2$, where m is the complex index of refraction and Q_{ext} and Q_{back} are referred to as the Mie extinction and backscatter efficiencies and may be explicitly calculated from a conventional scattering theory [12]. We also assume that the index of refraction is uniform for all wavelengths and particle sizes. We first work with a single known index of refraction and later include the index of refraction as a parameter to be retrieved.

The problem in question is to estimate the size distribution $n(r)$ from numerical values of $\hat{y}_i = y_i + \varepsilon_i$ as retrieved by the lidar channels, where ε_i represents an unknown deviation from the true values, which may be due to either random noise or systemic errors based on model deficiencies or assumptions. To reduce the degrees of freedom to a manageable size, it is necessary to describe the aerosol distribution in terms of a finite set of parameters. Two approaches are commonly employed. The first approach considers aerosol distributions to be comprised of only a few components with each having an analytic shape that only depends on a few parameters [13–15] in a nonlinear way, whereas the second approach is to express the distribution function as a linear combination of localized basis functions [16–21]. In the linearized approach, special care must be taken to stabilize the retrieval against instabilities arising from the ill-posed nature of the inversion. For example, Böckmann[16] used a truncated singular value decomposition, where the complex truncation criterion was based on the number of basis functions and the polynomial order of the basis functions. Müller *et al.* [17,18], Pahlow *et al.* [19], and Veselovskii *et al.* [20] approached stabilization using a Tikhonov regularization approach, but in such approaches, the smoothing parameters must be either guessed or obtained directly from the behavior of the retrieved solutions. It must be pointed out that all of these regularization methods tend to be nonrobust in the sense that a universal criterion for the optimization of a particular regularized inversion is unknown.

In this paper, we make use of a parameterized approach based on lognormal size distribution parameters. This has the virtue of being mathematically well posed and allows us to consider in a controlled way the information content of optical scattering coefficients. Notably, many of the qualitative results concerning the viability of different sensor channel configurations based on numerical tests are confirmed in this paper based on a more analytical framework.

To our knowledge, Bayesian statistics are not employed for the assessment of retrievals of aerosol size distributions from lidar measurements and are in fact replaced by an approach, which we describe as a forward Monte Carlo approach [13,20,21]. The forward Monte Carlo scheme can be described as follows: starting with a set of values for the optical coefficients, an ensemble of measurement vectors is obtained by adding errors from a random number generator to the original values. An ensemble of solutions is then obtained by performing the inverse method on the ensemble of measurement vectors, and the solution ensemble is examined to find its variances. Although to our knowledge it is not explicitly stated, we suppose that the rationale behind this method is that the ensemble of generated measurement vectors projected onto the range of the kernel is somehow representative of a statistical distribution of possible true measurement vectors. We show in Subsection 4.B that this is not generally correct when one considers the posterior error distribution that is conditional on the measured values.

In fact the forward Monte Carlo analysis answers the approximate question "if the true values of the optical coefficients are $\mathbf{y}$, what will be the statistical distribution of inversion results." This is useful in determining the overall performance of the inverse method but does not answer the question "if the result from a measurement is $\hat{\mathbf{y}}$, what is the statistical distribution of true aerosol distributions that could generate those measurement values." That is the question that should be answered in order to ascribe uncertainty to a solution associated with a particular instance of a measurement. It is a problem that is solved by Bayesian analysis in which the parameters to be determined, which are traditionally denoted by $\boldsymbol{\theta}$, are treated as random variables [22].

In the Bayesian framework the occurrence of a measurement is modeled as a two step sequence of realizations of random variables, and a posterior probability function that expresses the uncertainty of $\boldsymbol{\theta}$ is derived from this model. For the purposes in this paper we assume that the random variables can be modeled with PDFs. First the parameters $\boldsymbol{\theta}$ arise from an assumed prior PDF, $f_{\mathrm{pri}}(\boldsymbol{\theta})$. The prior PDF gives a statistical description of the probabilities of the parameters to be retrieved in the absence of any measurements and is based on prior assumptions including any constraints due to physical unrealizability. For example, with the requirement that the particle density of an aerosol distribution must be positive, one would choose a prior PDF whose values are zero over the region where the

particle density is negative. As another example, a prior PDF that is more heavily weighted at smoother aerosol distributions or distributions with lower total particle densities is implicit in the regularization schemes that are the basic building blocks of the inversion methods [17–20]. In fact the basic regularized inverse is a solution that is both the mean and maximum of the Bayesian posterior PDF with a prior PDF that has such properties [22]. After the realization of $\boldsymbol{\theta}$, the measurements $\hat{\mathbf{y}}$ then arise from the likelihood PDF, $f_{\mathrm{li}}(\hat{\mathbf{y}}|\boldsymbol{\theta})$ depending on the resulting $\boldsymbol{\theta}$. The posterior PDF is derived from the prior and likelihood PDFs by

$$f_{\mathrm{post}}(\boldsymbol{\theta}|\hat{\mathbf{y}}) = f_{\mathrm{li}}(\hat{\mathbf{y}}|\boldsymbol{\theta}) f_{\mathrm{pri}}(\boldsymbol{\theta}) / f_{\mathrm{marg}}(\hat{\mathbf{y}}), \tag{2}$$

where $f_{\mathrm{marg}}(\hat{\mathbf{y}})$ is the marginal PDF for the measurements without any constraint on $\boldsymbol{\theta}$. The marginal PDF is included in the formulation to normalize the posterior PDF, and is given by

$$f_{\mathrm{marg}}(\hat{\mathbf{y}}) = \int f_{\mathrm{li}}(\hat{\mathbf{y}}|\boldsymbol{\theta}) f_{\mathrm{pri}}(\boldsymbol{\theta}) \mathrm{d}\boldsymbol{\theta}. \tag{3}$$

The focus of this paper is to simplify the Bayesian inversion process by using a parametric aerosol model so that more sophisticate assessments of uncertainty can be efficiently implemented and compared to the more traditional forward Monte Carlo method. Unfortunately, a parameterized particle size distribution model may not be a physically realistic assumption. However, we feel that this trade-off is acceptable since many of the qualitative issues relating to the information content available for different optical coefficients should not be overly sensitive to the details describing the size distribution.

In Section 2 we describe the parameterization model and show how using a fractional error model can simplify the uncertainty assessment problem. In Section 3 we derive the formulas for calculating posterior PDFs with the fractional error model using only cross section density ratios so that the total particle number density is removed from the problem. In Section 4 we compare the results of the Bayesian and forward Monte Carlo analyses. Furthermore, we compare results of the forward Monte Carlo analyses using two different retrieval methods. In Section 5, we describe a procedure for determining credible sets of solutions from the posterior PDF with the index of refraction as an unknown parameter and will show results of the application of this procedure to diverse configurations of cross-section density measurements of different types (i.e., extinction or backscatter) and at different wavelengths. Our results are summarized in Section 6.

2. Methodologies

In this paper we restrict ourselves to the problem of retrieving a single mode lognormal distribution. In this case, the Fredholm integral equation becomes

$$y_i = \int_0^\infty K_i(r) N_0 \, n_{\mathrm{lognormal}}(r, \mathbf{p}) \mathrm{d}r = T_i(\mathbf{p}), \tag{4}$$

where N_0 represents the particle density. The $N_{\mathrm{lognormal}}$ is the normalized aerosol distribution function given by

$$n_{\mathrm{lognormal}}(r, \mathbf{p}) = \frac{1}{\sqrt{2\pi}\ln(\sigma) r} \exp\left(-\frac{\ln(r/\bar{r})^2}{2\ln(\sigma)^2}\right), \tag{5}$$

with $\mathbf{p}$ representing the lognormal parameters $(\bar{r}, \sigma)$, the median radius, and the geometric standard deviation (GSD). Solving the Fredholm equation then becomes a matter of finding the distribution parameters based on a nonlinear system of algebraic equations. The problem can be further simplified by working with ratios of measurements, eliminating N_0, and thus reducing the number of parameters by one [13,15]. However, in performing the Bayesian analysis, if N_0 is to remain eliminated from the problem, the error formulation must not have any dependence on it. This is most easily achieved by formulating the error in optical coefficients as a fractional error in the form

$$\hat{y}_i = y_i(1 + \delta_i). \tag{6}$$

In this paper we use the ^ symbol to indicate that a coefficient is disturbed by measurement error, whereas true values remain unmarked. Considering a ratio of measured coefficients, which are independent of N_0, we have

$$\hat{R}_k = \frac{y_i(1+\delta_i)}{y_j(1+\delta_j)} = R_k\left(1 + \frac{1+\delta_i}{1+\delta_j} - 1\right) = R_k(1+\varepsilon_k), \tag{7}$$

where R_k is the ratio of true optical coefficients y_i/y_j, thus allowing the ratio error to have the same parameter-independent fractional error formulation as the optical coefficients, where the fractional error of the ratio has the form

$$\varepsilon_k = (1+\delta_i)/(1+\delta_j) - 1. \tag{8}$$

3. Bayesian Analysis

In this section, we derive the formula for calculating the posterior probability function in Eq. (2) with measured ratios $\hat{\mathbf{R}}$ and size parameters $\mathbf{p}$ replacing the $\hat{\mathbf{y}}$ and $\boldsymbol{\theta}$, respectively. The likelihood PDF is derived from the ratio error PDF

$$f_{\mathrm{li}}(\hat{\mathbf{R}}|\mathbf{p}) = f_\varepsilon[\varepsilon(\hat{\mathbf{R}}, \mathbf{p})] \mathbf{J}_{\varepsilon/\hat{\mathbf{R}}}(\hat{\mathbf{R}}, \mathbf{p}), \tag{9}$$

where f_ε represents the PDF for the error distribution, and $\mathbf{J}_{\varepsilon/\hat{\mathbf{R}}}(\hat{\mathbf{R}})$ represents the differential volume transformation function given by the determinant of the Jacobian matrix [23], i.e.,

$$\mathbf{J}_{\varepsilon/\hat{\mathbf{R}}} = \left|\det\left(\frac{\partial\varepsilon}{\partial\hat{\mathbf{R}}}\right)\right|, \tag{10}$$

where $\partial\varepsilon/\partial\hat{\mathbf{R}}$ is shorthand for the matrix

$$\frac{\partial\varepsilon}{\partial\hat{\mathbf{R}}} = \begin{pmatrix} \partial\varepsilon_1/\partial\hat{R}_1 & \cdots & \partial\varepsilon_1/\partial\hat{R}_N \\ \vdots & \ddots & \vdots \\ \partial\varepsilon_N/\partial\hat{R}_1 & \cdots & \partial\varepsilon_N/\partial\hat{R}_N \end{pmatrix}. \tag{11}$$

The form of $\varepsilon(\hat{\mathbf{R}}, \mathbf{p})$ is easily derived from Eq. (7) as

$$\varepsilon_i = \frac{\hat{R}_i}{R_i(\mathbf{p})} - 1, \tag{12}$$

resulting in a diagonal matrix in Eq. (11) and therefore

$$\mathbf{J}_{\varepsilon/\hat{\mathbf{R}}}(\hat{\mathbf{R}}, \mathbf{p}) = \prod_i \frac{1}{R_i(\mathbf{p})}. \tag{13}$$

To derive the formula for the ratio error PDF, $f_\varepsilon(\varepsilon)$, we begin by establishing the set of ratios of the N optical coefficients as

$$R_i = y_i/y_N, \qquad i \in \{1, \ldots, N-1\}. \tag{14}$$

The relationship between the ratio error and optical coefficient error was already given in Eq. (8), but to derive the ratio error PDF, $f_\varepsilon(\varepsilon)$, from the optical coefficient error PDF, $f_\delta(\delta)$, the dimension of the error vector must be maintained, which we do by using an extended ratio error vector by appending the Nth optical coefficient error to the ratio error vector so that

$$\varepsilon_i = \begin{cases} \frac{1+\delta_i}{1+\delta_N} - 1, & i \neq N \\ \delta_N, & i = N \end{cases},$$

and by inverting these formulas we obtain

$$\delta_i = \begin{cases} \varepsilon_i + \varepsilon_N + \varepsilon_i\varepsilon_N, & i \neq N \\ \varepsilon_N, & i = N \end{cases}. \tag{16}$$

The PDF of the extended ratio error vector ε' is given by

$$f_{\varepsilon'}(\varepsilon') = f_\delta(\delta(\varepsilon'))\mathbf{J}_{\delta/\varepsilon'}(\varepsilon'), \tag{17}$$

and the matrix elements needed for $\mathbf{J}_{\delta/\varepsilon'}(\varepsilon')$ are derived from Eq. (16) as

$$\frac{\partial\delta}{\partial\varepsilon'} = \begin{pmatrix} 1+\varepsilon_N & 0 & \cdots & 0 & 1+\varepsilon_1 \\ 0 & 1+\varepsilon_N & \cdots & 0 & 1+\varepsilon_2 \\ \vdots & \vdots & \ddots & \vdots & \vdots \\ 0 & 0 & \cdots & 1+\varepsilon_N & 1+\varepsilon_{N-1} \\ 0 & 0 & \cdots & 0 & 1 \end{pmatrix}, \tag{18}$$

Therefore, the expression for the differential volume transformation is finally calculated as

$$\mathbf{J}_{\delta/\varepsilon'}(\varepsilon') = |(1+\varepsilon_N)^{N-1}|. \tag{19}$$

The fractional errors of the optical coefficients are assumed to have a Gaussian distribution and to be independent having standard deviations σ_i, which leads directly to the following formula for the extended ratio error vector PDF

$$f_{\varepsilon'}(\varepsilon') = \frac{1}{(2\pi)^{N/2}\prod_{i=1}^N \sigma_i} \times \exp\left(-\frac{1}{2}\left[\sum_{i=1}^{N-1}\frac{(\varepsilon_i + \varepsilon_N + \varepsilon_i\varepsilon_N)^2}{\sigma_i^2} + \frac{\varepsilon_N^2}{\sigma_N^2}\right]\right) \times |(1+\varepsilon_N)^{N-1}|. \tag{20}$$

Once the PDF in the extended space is obtained, we can project the PDF onto the correct subspace by analytically integrating $f_{\varepsilon'}(\varepsilon')$ over ε_N to get $f_\varepsilon(\varepsilon)$, the PDF of the nonextended error vector. Expressing the argument of the exponential function as $-0.5[A(\varepsilon_N - B)^2 + C]$ and making the substitution $u = \varepsilon_N + B$, results in the following expression:

$$f_\varepsilon(\varepsilon) = \frac{1}{(2\pi)^{N/2}\prod_{i=1}^N \sigma_i}\exp\left(-\frac{1}{2}C\right) \times \int_{-\infty}^{\infty}\exp\left(-\frac{1}{2}Au^2\right)|(1-B+u)^{N-1}|\mathrm{d}u, \tag{21}$$

where A, B, and C are functions of ε given by

$$A = \frac{1}{\sigma_N^2} + \sum_{i=1}^{N-1}\frac{1+2\varepsilon_i+\varepsilon_i^2}{\sigma_i^2}, \tag{22a}$$

$$B = \frac{\sum_{i=1}^{N-1}(\varepsilon_i + \varepsilon_i^2)/\sigma_i^2}{A}, \tag{22b}$$

$$C = \sum_{i=1}^{N-1}\frac{\varepsilon_i^2}{\sigma_i^2} - AB^2. \tag{22c}$$

Direct integration gives

$$f_\varepsilon(\varepsilon) = \frac{\exp\left(-\frac{1}{2}C\right)\sum_{k=0}^{N-1}\left(\sqrt{\frac{2}{A}}\right)^{k+1}(1-B)^{N-1-k}\binom{N-1}{k}\left[I_k(\infty) + I_k(-\infty) - 2I_k\left(\sqrt{\frac{A}{2}}(B-1)\right)\right]}{(2\pi)^{N/2}\prod_{i=1}^N \sigma_i}, \tag{23}$$

where

$$I_k(u) = \int_0^u x^k \exp(-x^2)\mathrm{d}x, \tag{24}$$

which can be evaluated recursively with

$$I_{k+2}(u) = \frac{1}{2}[(k+1)I_k(u) - u^{k+1}\exp(-u^2)], \tag{25a}$$

where

$$I_0(u) = \frac{1}{2}\pi \mathrm{erf}(u), \tag{25b}$$

$$I_1(u) = \frac{1}{2}[1 - \exp(-u^2)]. \tag{25c}$$

With this formulation, we can now calculate the likelihood function in Eq. (9). In our calculations, we assume that the prior PDF is uniform over the domain of the distribution parameter values, where we have tabulated the optical coefficients and zero elsewhere so that the posterior PDF is simply calculated by numerically integrating over the distribution parameter domain.

4. Comparisons

A. Simulations

In a typical multiwavelength Nd:YAG laser lidar system the optical coefficients that are obtained include the volume backscatter at 1064, 532, and 355 nm. However, previous work [18] has shown that backscatter coefficients are not sufficient to obtain microphysical parameters when the refractive index is unknown and extinction measurements are critical. Therefore, extra nitrogen Raman channels at 607 and 387 nm are included in the receiver, which provide independent measurements of the aerosol extinction at 532 and 355 nm. This $(3\beta + 2\alpha)$ configuration is taken to be the reference system to which other systems can be compared.

To begin, we first perform calculations based on the forward Monte Carlo assessment. In this scheme, the measurement vector ensembles are numerically generated according to the statistical model governing the noise impressed on the optical data. For each ensemble element, a retrieval of the parameter vector is obtained based on a particular choice of the inversion scheme. Finally, the statistics of the resultant retrieved parameter vector ensembles can be evaluated and compared.

Our retrieval methods are implemented by searching a table derived from optical coefficients computed over a grid of particle median radii and GSDs. For our computational grid, the median radius discretization is divided into two segments with the first segment being 42 points logarithmically spaced from 10 to 50 nm. The second segment ranges from 50 nm to 1 μm in increments of 2 nm. The GSD discretization was from 1.1 to 2.4 in increments of 0.002.

In performing the inversion of the measurement data, we used two retrieval methods. In the first method, distribution parameters were retrieved by finding the $\mathbf{p}$ that minimizes the maximum deviation $\Delta(\mathbf{p})$ among the measurement ratios R_i, i.e.,

$$\Delta(\mathbf{p}) = \max_i \left\{ \left| \frac{R_i(\mathbf{p})}{\hat{R}_i} - 1 \right| \right\} \tag{26}$$

We will refer to this first method as the minimized maximum deviation (MMD) method. In the second retrieval method, distribution parameters were retrieved by finding the $\mathbf{p}$ that maximizes the posterior PDF as described in Section 3. The computation time for the maximized posterior probability density function (MPPDF) method was substantially greater than in the MMD method, so we reduced the median radius and GSD grids by excluding alternating grid points in both dimensions.

Once the calculations were performed, the metrics we use to quantify the differences between the uncertainty assessments were the marginal cumulative distribution functions (CDFs) in both the median radius and GSD. For the remainder of this paper, when discussing posterior PDFs or CDFs we will omit the "post" subscript and the $\hat{\mathbf{R}}$ in $f_{\mathrm{post}}(\theta|\hat{\mathbf{R}})$ for the sake of clarity and use subscripts to denote a specific parameter or subset of parameters. For the Bayesian assessment in this two parameter model, the marginal CDF is derived from the posterior PDF as

$$F_X(x) = \int_{X_{\min}}^{x} \int_{Y_{\min}}^{Y_{\max}} f_{X,Y}(x', y')\mathrm{d}y'\mathrm{d}x', \tag{27}$$

with X representing the lognormal distribution parameter that is being considered, either $\bar{r}$ or σ, and Y representing the other parameter. The CDFs for the two forward Monte Carlo assessments were estimated from the ensemble of retrieval outcomes by the formula

$$\hat{F}_X(x) = N\{X \le x\}/N_{\mathrm{total}}, \tag{28}$$

where $N\{X \le x\}$ represents the number of ensemble members with the distribution parameter under consideration less than or equal to x and N_{total} represents the total number of ensemble members.

Synthetic measurements of optical coefficients used as inputs to the forward Monte Carlo assessments for comparison were created over a grid representing true particle size distributions with median radii varying from 0.2 to 0.8 μm in steps of 0.05 μm and the GSD varying from 1.3 to 2.1 in steps of 0.05. The optical coefficient error was modeled as in Eq. (6) with each δ_i being zero mean Gaussian distributed with a standard deviation of 0.1. In this analysis we are working with a five-dimensional

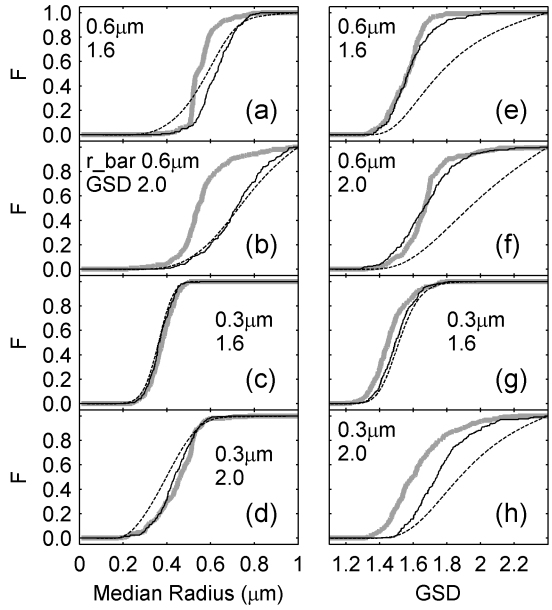

Fig. 1. (a)–(d) CDFs of retrieved median radius and (e)–(h) GSD with modeled true distribution parameters $(\bar{r}, \sigma)$ of: (a), (e) $(0.6\,\mu\mathrm{m}, 1.6)$; (b), (f) $(0.6\,\mu\mathrm{m}, 2)$; (c), (g) $(0.3\,\mu\mathrm{m}, 1.6)$; (d), (h) $(0.3\,\mu\mathrm{m}, 2)$. The dotted curves represents the Bayesian posterior CDF. The thin black curves represent the estimated CDF using MPPDF retrievals. The thick gray curves represent the estimated CDF using MMD retrievals.

optical coefficient vector used to retrieve a three-parameter aerosol model, therefore real measurements with errors would not be in the range of optical coefficient vectors that correspond to aerosol parameters. To avoid any possible effects with this issue, a single error vector, δ_0, was generated with five samples drawn from a Gaussian random number generator with the same statistical properties as in the error model. This error vector was used to disturb the simulated true optical coefficients using Eq. (6) for each grid point. Figure 1 shows some examples of the CDFs derived from the forward Monte Carlo methods compared with the Bayesian analytical CDFs. Examples of two-dimensional scatterplots are shown superimposed on the Bayesian PDF contours in Fig. 2. We note that there are substantial discrepancies between the forward Monte Carlo estimated CDFs and the Bayesian CDFs and give an explanation of this result in Subsection 4.B after giving a theoretical discussion of error PDFs.

The differences in uncertainty between the forward Monte Carlo and Bayesian assessments were quantified using a deviation parameter

$$(\mathrm{dev}\,X)_{\mathrm{meth}} = \int |F_X(x) - \hat{F}_{X,\mathrm{meth}}(x)|\mathrm{d}x, \qquad (29)$$

where $F_X(x)$ represents the Bayesian CDF and "meth" represents the retrieval method used in the forward Monte Carlo assessment. Figure 3 shows images of the deviation parameter for both the

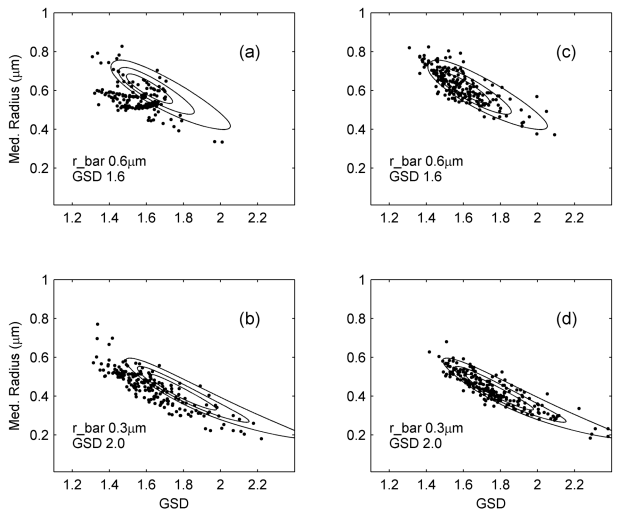

Fig. 2. Scatterplots of forward Monte Carlo outcomes with contours of Bayesian PDFs. Outcomes using MMD retrievals are shown in (a) and (b). MPPDF retrievals are shown in (c) and (d). The modeled true distribution parameters, $(\bar{r}, \sigma)$, are (a), (c) $(0.6\,\mu\mathrm{m}, 1.6)$, [corresponding to Figs. 1(a) and 1(e)], and (b), (d) $(0.3\,\mu\mathrm{m}, 2)$, [corresponding to Figs. 1(d) and 1(h)].

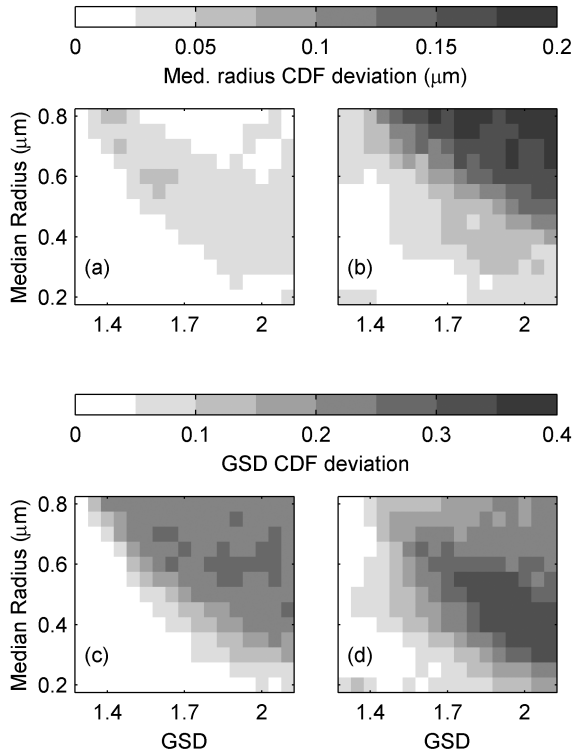

Fig. 3. (a), (b) Median radius and (c), (d) GSD CDF deviation from the Bayesian CDF as formulated in (29) using the (a), (c) MPPDF and (b) (d) MMD retrieval methods.

MPPDF and MMD retrieval methods. Clearly, there are significant differences between the forward Monte Carlo assessment with the proper Bayesian assessment in both implementations. They also show that the forward Monte Carlo method using MPPDF

retrievals generally gives an uncertainty assessment closer to the Bayesian assessment than when using MMD retrievals. To show that this is a general trend, we performed the deviation parameter calculations for four other δ_0 error vectors as shown in Table 1. These data show that for each δ_0, the majority of the computed deviation parameters are larger when using the MMD retrieval method than with the MPPDF retrieval method for both the median radius and GSD. Furthermore, considering all δ_0's combined, 66.2% of the computations among the different δ_0's and modeled true parameters show an increase in the median radius CDF deviation by more than a factor of 2. We also note that the variation of results shown in Table 1 clearly shows the need for the use of the δ_0's.

B. Discussion

We attribute the differences in the Bayesian assessment from the forward Monte Carlo assessments to a subtle consequence of the transformation between joint probability domains, which is that, even if measurement error probabilities are independent from underlying parameters in the forward model, their posterior probabilities conditional to the measurements will have a different PDF than the one in the forward model. To see how this arises, we consider the joint PDF in the error vector and aerosol distribution parameter vector, $(\varepsilon, \boldsymbol{\theta})$ given by

$$f_{\varepsilon,\theta}(\varepsilon,\theta) = f_{\varepsilon}(\varepsilon) f_{\theta}(\theta), \tag{30}$$

so that measurement errors are statistically independent of $\boldsymbol{\theta}$. From this PDF we obtain the PDF in the domain of coefficient true values and measurement errors, $(\varepsilon, \mathbf{y})$. For the given error-free coefficient values, we assume there is a unique inverse, $\boldsymbol{\theta} = \mathbf{T}^{-1}(\mathbf{y})$, giving the corresponding aerosol distribution parameters, so that the PDF in $(\varepsilon, \mathbf{y})$ is $f_{\varepsilon}(\varepsilon) f_{\theta}[\mathbf{T}^{-1}(\mathbf{y})]\mathbf{J}_{\theta/\mathbf{y}}(\mathbf{y})$, where $\mathbf{J}_{\bullet/\bullet}$ represents the differential volume transformation as defined in Eqs. (10) and (11).

We now repeat this process by obtaining the PDF in measurement errors and measured values, $(\varepsilon, \hat{\mathbf{y}})$. Using the fact that the measurement true values can be derived from measured values and measurement errors by an analytic function $\mathbf{y} = \mathbf{M}^{-1}(\hat{\mathbf{y}}, \varepsilon)$, then the PDF in this domain is

$$f_{\varepsilon,\hat{\mathbf{y}}}(\varepsilon,\hat{\mathbf{y}}) = f_{\varepsilon}(\varepsilon) f_{\theta}\{\mathbf{T}^{-1}[\mathbf{M}^{-1}(\hat{\mathbf{y}},\varepsilon)]\} \times \mathbf{J}_{\theta/\mathbf{y}}[\mathbf{M}^{-1}(\hat{\mathbf{y}},\varepsilon)]\mathbf{J}_{\mathbf{y}/\hat{\mathbf{y}}}(\hat{\mathbf{y}},\varepsilon). \tag{31}$$

[Note that $\mathbf{M}^{-1}(\hat{\mathbf{y}}, \varepsilon)$ would typically be very straightforward; e.g., from Eq. (6) one would have $y_i = \hat{y}_i/(1+\varepsilon_i)$.] The conditional error PDF, $f_{\varepsilon|\hat{\mathbf{y}}}(\varepsilon|\hat{\mathbf{y}})$, is simply $f_{\varepsilon,\hat{\mathbf{y}}}(\varepsilon,\hat{\mathbf{y}})$ multiplied by the normalizing constant for a given $\hat{\mathbf{y}}$. Hence we can see from Eq. (31) that differences in $f_{\varepsilon|\hat{\mathbf{y}}}(\varepsilon|\hat{\mathbf{y}})$ and $f_{\varepsilon}(\varepsilon)$ arise from any of the following three contributing factors which are: (1) from $f_{\theta}\{\mathbf{T}^{-1}[\mathbf{M}^{-1}(\hat{\mathbf{y}},\varepsilon)]\}$ if the prior aerosol parameter PDF is nonuniform, (2) from $J_{\theta/\mathbf{y}}[\mathbf{M}^{-1}(\hat{\mathbf{y}},\varepsilon)]$ if there is a nonlinear relationship between aerosol distribution parameters and measurement true values, and (3) from $\mathbf{J}_{\mathbf{y}/\hat{\mathbf{y}}}(\hat{\mathbf{y}},\varepsilon)$ if the error model is nonadditive.

The second condition is present in our analyses due to the nonlinear nature of the lognormal particle size distribution parameterization. Reviewing Fig. 1, the fact that larger discrepancies between the forward estimated Monte Carlo and the Bayesian CDFs are associated with higher uncertainties is indicative of this condition. It is worthwhile to note that it may be possible to yield smaller uncertainties by including a prior PDF into the Bayesian formulation based on statistical properties of aerosols determined from long term direct measurements. However, in this study we do not use such data and therefore consider the prior PDF to be uniform within the bounds of the lookup table. In current methods based on regularization [17–20], a nonuniform prior PDF is implicit by favoring smoother solutions.

The fractional error model that we use makes the third condition present. Alternatively the fractional error model could be viewed as a parameter-dependent error distribution, specifically an additive Gaussian distributed error with a standard deviation proportional to the true optical coefficient of the aerosol distribution. In advocating the usefulness of the Bayesian methods, we note that if a nonindependent error formulation were used, Eq. (30) would be $f_{\varepsilon,\theta}(\varepsilon,\theta) = f_{\varepsilon}(\varepsilon|\boldsymbol{\theta}) f_{\theta}(\boldsymbol{\theta})$. In that case a forward Monte

Table 1. CDF Deviation Comparison

	Median Radius Deviation Ratio[a] Threshold		GSD Deviation Ratio[b] Threshold	
	1.0	2.0	1.0	2.0
Error Vector, δ_0	Percent Above Threshold			
1	95.0	60.2	70.6	38.5
2	95.9	74.7	51.6	26.2
3	90.0	63.3	100	67.9
4	89.6	60.6	69.2	46.2
5	93.7	71.9	57.9	36.2
All combined	92.9	66.2	69.9	43.0

[a]Ratio of MMD to MPPDF deviation parameters $(\mathrm{dev}_{\bar{r}})_{\mathrm{MMD}}/(\mathrm{dev}_{\bar{r}})_{\mathrm{MPPDF}}$.
[b]$(\mathrm{dev}_{\sigma})_{\mathrm{MMD}}/(\mathrm{dev}_{\sigma})_{\mathrm{MPPDF}}$.

Carlo computation would not be feasible since one would not have θ available to be able to implement a random error generator. To our knowledge these issues have not been addressed in the context of inferring an aerosol distribution uncertainty from lidar measurements.

5. Applications to Unknown Index of Refraction

The posterior PDF can be used to assess uncertainty by deriving regions S that have a specific credibility (i.e., *a posteriori* probability), C_0. In two dimensions a family of sets can be defined as the regions enclosed by contours of $f(\mathbf{p}) = L$,

$$S(L) = \{\mathbf{p} : f(\mathbf{p}) \geq L\}, \tag{32}$$

corresponding to different values of L [Note that this is a departure from the conventional notation in the sense that $S(L)$ refers to a function that maps the set of real numbers into the family of all subsets of the entire parameter domain.] This defines credibility as a function of L by

$$C(L) = \int_{S(L)} f(\mathbf{p})\mathrm{d}\mathbf{p}, \tag{33}$$

and a credible set can be found as $S(L_0)$ with L_0 such that $C(L_0) = C_0$. Sets found this way have the property of being the optimal credible set in the sense that they are sets with the least total area. Although other properties that might be of interest are not necessarily satisfied, such as connectedness or the credible set having the least maximum distance among the points of the set, these issues are beyond the scope of this paper.

With the inclusion of the complex index of refraction, $\mathbf{m} = (m_{\mathrm{Re}}, m_{\mathrm{Im}})$, as unknown parameters, credible sets derived as from Eq. (32) in the full four-dimensional domain are not easily visualized. To arrive at an optimal credibility set in the four-dimensional case, we use the following approach. First, a continuum of sets on each subdomain $S_{\mathbf{p}}(L_{\mathbf{p}})$, and $S_{\mathbf{m}}(L_{\mathbf{m}})$ are obtained based on the two-dimensional approach, except suitable marginal PDFs are used instead of the full four-dimensional PDF, i.e.,

$$S_{\mathbf{p}}(L_{\mathbf{p}}) = \{\mathbf{p} : f_{\mathbf{p}}(\mathbf{p}) \geq L_{\mathbf{p}}\}, \tag{34a}$$

$$S_{\mathbf{m}}(L_{\mathbf{m}}) = \{\mathbf{m} : f_{\mathbf{m}}(\mathbf{m}) \geq L_{\mathbf{m}}\}, \tag{34b}$$

where

$$f_{\mathbf{p}}(\mathbf{p}) = \int_{\Omega_{\mathbf{m}}} f_{\mathbf{p},\mathbf{m}}(\mathbf{p},\mathbf{m})\mathrm{d}\mathbf{m}, \tag{35a}$$

$$f_{\mathbf{m}}(\mathbf{m}) = \int_{\Omega_{\mathbf{p}}} f_{\mathbf{p},\mathbf{m}}(\mathbf{p},\mathbf{m})\mathrm{d}\mathbf{p}, \tag{35b}$$

where $\Omega_{\mathbf{p}}$ and $\Omega_{\mathbf{m}}$ represent the entire subdomains of size parameters and indexes of refraction, respectively. Next, for each choice of $(L_{\mathbf{p}}, L_{\mathbf{m}})$, the credibility may be calculated as

$$C(L_{\mathbf{p}}, L_{\mathbf{m}}) = \int_{S_{\mathbf{p}}(L_{\mathbf{p}})\times S_{\mathbf{m}}(L_{\mathbf{m}})} f_{\mathbf{p},\mathbf{m}}(\mathbf{p},\mathbf{m})d\mathbf{p}d\mathbf{m} \tag{36}$$

with $C(L_{\mathbf{p}}, L_{\mathbf{m}})$ monotonically decreasing in both $L_{\mathbf{p}}$ and $L_{\mathbf{m}}$. The solution to $C(L_{\mathbf{p}}, L_{\mathbf{m}}) = C_0$ is a contour in $(L_{\mathbf{p}}, L_{\mathbf{m}})$ rather than a single point. The credible set is chosen from the $L_{\mathbf{p}}$ and $L_{\mathbf{m}}$ values on the contour that minimize $A_{\mathbf{p}}A_{\mathbf{m}}$, where $A_{\mathbf{p}}$ and $A_{\mathbf{m}}$ represent the areas of $S_{\mathbf{p}}(L_{\mathbf{p}})$ and $S_{\mathbf{m}}(L_{\mathbf{m}})$, respectively.

In implementing this method, the median radius grid was divided into three segments with the first segment being 25 points logarithmically spaced from 2 to 20 nm. The second segment ranged from 20 to 200 nm in increments of 2 nm. The third segment ranged from 200 to 900 nm in increments of 10 nm. The GSD grid was divided into two segments with the first segment being 21 points ranging from 1.074 to 1.200 such that σ-1 was logarithmically spaced and the second segment ranging from 1.2 to 2.4 in increments of 0.01. The method was applied to simulated measurements with true distribution parameters of $(\bar{r}, \sigma, m_{\mathrm{Re}}, m_{\mathrm{Im}}) = (0.3\,\mu\mathrm{m},\ 1.4,\ 1.5,\ -0.03)$ with the errors described in Eq. (6) with 10% standard deviation. This was repeated for five possible measurement configurations delineated in Table 2.

An example of the total set volume minimization procedure can be seen in Fig. 4, where the total set volume, $A_{\mathbf{p}}A_{\mathbf{m}}$, is plotted versus $A_{\mathbf{m}}$ with a 90% credibility being specified. The minimum values on the plots represent the optimal trade-off between

Table 2. Measurement Groups

Group Index	Backscatter λ (nm)								Extinction λ (nm)	
	355	400	416	532	683	710	800	1064	355	532
1	×	×		×		×	×	×	×	×
2	×			×				×	×	×
3	×			×				×	×	
4	×	×	×	×	×	×	×	×		
5	×			×				×		

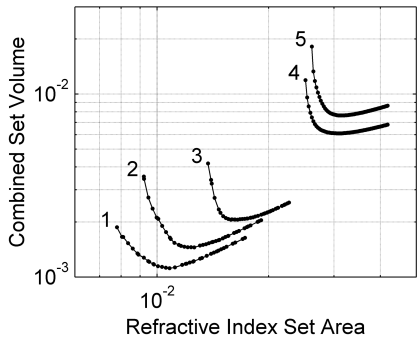

Fig. 4. $A_{\mathbf{p}}A_{\mathbf{m}}$ versus $A_{\mathbf{m}}$ of sets with 90% credibility for five measurement groups.

the uncertainty in size parameters and an index of refraction. As the set in one subdomain decreases, the set in the other subdomain must increase to maintain the same credibility level. The minimal set in one subdomain occurs when the set in the other subdomain is the entire subdomain. We refer to this minimal set as the individual credible set. These are represented in Fig. 4 as the end points of the plots, the leftmost and rightmost points representing the individual credible sets for an index of refraction and size parameters, respectively. The points where the plots have minimum values represent the optimal four-dimensional credible set, and we refer to the sets in the subdomains as the simultaneous sets. The resulting credible set components are shown in Fig. 5 showing the importance of the extinction measurements when not assuming an index of refraction. Comparing Figs. 5(a) and 5(f) with Figs. 5(c) and 5(h) demonstrates that the inclusion of only one extinction measurement with three backscatter measurements results in a decrease in uncertainty that is clearly more substantial than improvements in uncertainty that would result from including five additional backscatter measurements as seen in Figs. 5(b) and 5(g). These results are in qualitative agreement with previous studies carried out with regularization [18]. The band structure seen in the index of refraction credible sets has been demonstrated by several authors [16,24] based on regularization approaches. However, in our case we are able to connect this structure directly to the posterior probability.

6. Conclusion

We have presented a Bayesian approach to uncertainty assessment. This method allows us to calculate the probability that a given aerosol size distribution will occur and will result in an optical data vector, which is consistent with the measurements. This approach is quite different from the forward Monte Carlo method, and choosing which method to use depends on the context in which the uncertainty analysis is to be applied. However, when making an inference about an unknown aerosol size distribution, the Bayesian approach is the appropriate choice as previously demonstrated through an intercomparison with a cumbersome reverse Monte Carlo method [25]. The reader should not assume that all Monte Carlo methods should be avoided when taking a Bayesian approach. The forward Monte Carlo method is very simple, and there are more sophisticated ones that are indeed used for Bayesian analysis [26,27].

We have derived a PDF for the distribution of errors for any number of optical coefficient ratios under the reasonable assumption that the fractional errors in the optical coefficients are constant. This was done to remove the total particle number as a parameter for retrieval and thereby reducing the dimension of aerosol distribution parameters so that a Bayesian treatment of the inverse problem could be implemented more efficiently. Using the analytical formulation of the PDF, we implemented a Bayesian approach to the assessment of uncertainty of unknown aerosol size distributions and showed that significant deviations occur compared to when the forward Monte Carlo method is used. In fact, we show that the measurement error PDF takes a different form when the information present in the

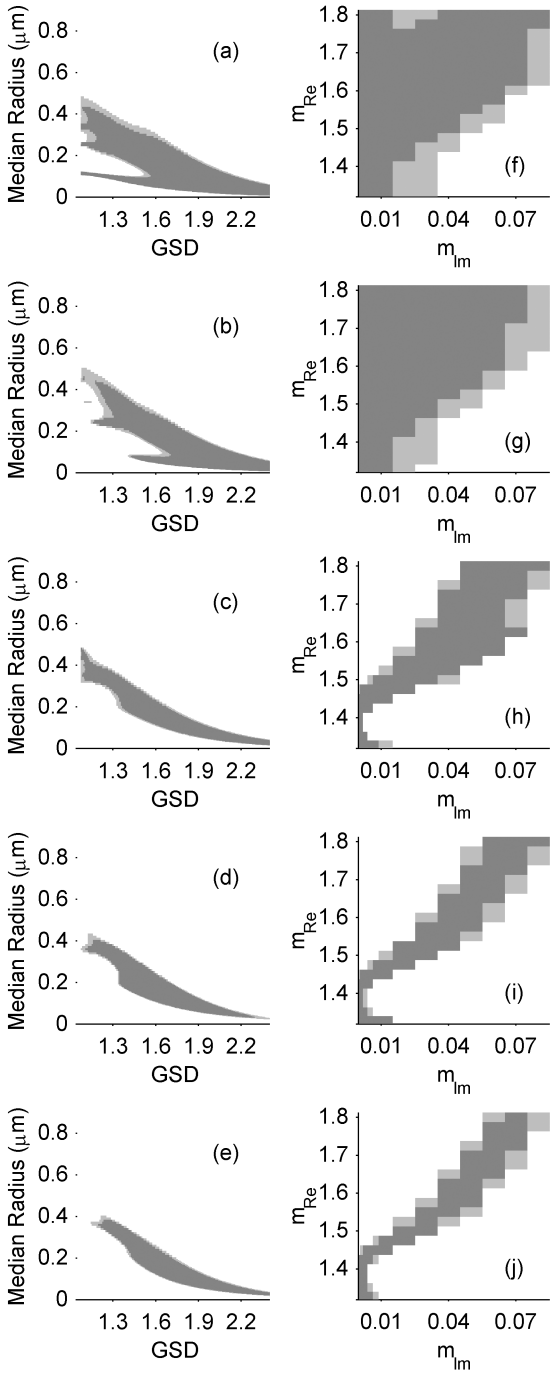

Fig. 5. Individual (dark gray area) and simultaneous (dark gray + light gray area) sets of 90% credibility for measurement groups (a), (f) 5, (b), (g) 4, (c), (h) 3, (d) (i) 2, and (e), (j) 1.

measurements is considered and any of a number of common nonideal conditions are met. Two of these conditions, which were present in this study are (a) nonlinear relationships between retrieval parameters and the underlying optical coefficient values, and (b) measurement error PDFs that are dependent on the retrieval parameters.

When the two approaches were compared, we found that the Bayesian analysis resulted in larger uncertainties in comparison with the forward Monte Carlo method. However, we note that it is conceivable that uncertainty could be reduced if a nonuniform prior PDF were to be incorporated into the Bayesian formulation.

The Bayesian technique was then used to retrieve credible sets for the combined set of aerosol distribution parameters including both size distribution and complex refractive index over a variety of optical coefficient scenarios. In particular, with the index of refraction considered to be unknown, we demonstrated the necessity of combining extinction and backscatter measurements. In fact, the addition of only a single extinction measurement to the traditional three backscatter retrievals substantially decreased the uncertainty when compared to an alternate scenario, where only additional backscatter measurement was available. We also note that many of the qualitative results that had been obtained using linear regularization based methods are also seen in the Bayesian framework. Specifically, there were similarities in the results regarding the structure of the sets of complex index of refraction in the retrieval domain and the effects that different channel configurations have on aerosol distribution uncertainty.

Finally, we point out that the Bayesian approach is clearly applicable to bimodal distributions except for the fact that the subsequent increase in the dimensionality of the parameter space would make computation times unreasonable with the basic numeric integration methods employed for this paper. To overcome these difficulties, we are currently considering methods that use the Metropolis–Hastings Markov chain Monte Carlo algorithm for generating samples congruent with multidimensional PDFs that could be computed in the Bayesian framework [26,27].

We thank the two anonymous reviewers who gave many useful suggestions, which we believe have improved the quality of this paper. This work is partially supported under grants from the National Oceanic and Atmospheric Administration (NOAA) NA17AE1625 and NASA NCC-1-03009.

References

1. R. J. Charlson, S. E. Schwartz, J. M. Hales, R. D. Cess, J. A. Coakley, J. E. Hansen, and D. J. Hofmann, "Climate forcing by antropogenic aerosol," Science **255**, 423–430 (1992).
2. J. A. Coakley and R. D. Cess, "Response of the NCAR community climate model to the radiative forcing by the naturally occurring tropospheric aerosols," J. Atmos. Sci. **42**, 1677–1692 (1985).
3. G. E. Shaw, "Inversion of optical scattering and spectral extinction measurements to recover aerosol size spectra," Appl. Opt. **18**, 988–993 (1979).
4. N. T. O'Neill and J. R. Miller, "Combined solar aureole and solar beam extinction measurements: 2. Studies of the inferred aerosol size distributions," Appl. Opt. **23**, 3697–3703 (1984).
5. D. Tanre, C. Devaux, M. Herman, R. Santer, and J. Y Gac, "Radiative properties of desert aerosols by optical ground based measurements at solar wavelengths," J. Geophys. Res. **93**, 14223–14231 (1988).
6. G. Tonna, T. Nakajima, and R. Rao, "Aerosol features retrieved from solar aureole data: a simulation study concerning a turbid atmosphere," Appl. Opt. **34**, 4486–4499 (1995).
7. T. Nakajima, G. Tonna, R. Rao, P. Boi, Y. Kaufman, and B. Holben, "Use of sky brightness measurements from ground for remote sensing of particulate polydispersions," Appl. Opt. **35**, 2672–2686 (1996).
8. M. D. King, D. M. Byrne, B. M. Herman, and J. A. Reagan, "Aerosol size distributions obtained by inversion of spectral optical depth measurements," J. Atmos. Sci. **35**, 2153–2167 (1978).
9. R. A. Ferrare, S. H. Melfi, D. N. Whiteman, and K. D. Evans, "Raman lidar measurements of Pinatubo aerosols over southeastern Kansas during November–December 1991," Geophys. Res. Lett. **19**, 1599–1602 (1992).
10. R. A. Ferrare, S. H. Melfi, D. N. Whiteman, K. D. Evans, M. Poellot, and Y. J. Kaufman, "Raman lidar measurements of aerosol extinction and backscattering 2. Derivation of aerosol real refractive index, single-scattering albedo, and humidification factor using Raman lidar and aircraft size distribution measurements," J. Geophys. Res. **103**, 19673–19690 (1998).
11. D. Althausen, D. Müller, A. Ansmann, U. Wandinger, H. Hube, E. Clauder, and S. Zörner, "Scanning 6-wavelength 11-channel aerosol lidar," J. Atmos. Ocean. Technol. **17**, 1469–1482 (2000).
12. C. F. Bohren and D. R. Huffman, *Absorption and Scattering of Light by Small Particles* (Wiley, 1983).
13. B. R. Herman, B. Gross, F. Moshary, and S. Ahmed, "Extension of the graphical technique for estimation of particle size distribution parameters for the consistent intercomparison of diverse sets of multiwavelength lidar derived optical coefficients," Appl. Opt. **44**, 6462–6473 (2005).
14. B. R. Lienert, J. N. Porter, and S. K. Sharma, "Repetitive genetic inversion of optical extinction data," Appl. Opt. **40**, 3476–3482 (2001).
15. M. D. Post, "A graphical technique for retrieving size distribution parameters from multiple measurements: visualization and error analysis," J. Atmos. Oceanic Technol. **13**, 863–869 (1996).
16. C. Böckmann, "Hybrid regularization method for the ill-posed inversion of multiwavelength lidar data in the retrieval of aerosol size distributions," Appl. Opt. **40**, 1329–1342 (2001).
17. D. Müller, U. Wandinger, and A. Ansmann, "Microphysical particle parameters from extinction and backscatter lidar data by inversion with regularization: theory," Appl. Opt. **38**, 2346–2357 (1999).
18. D. Müller, U. Wandinger, and A. Ansmann, "Microphysical particle parameters from extinction and backscatter lidar data by inversion with regularization: simulation," Appl. Opt. **38**, 2358–2368 (1999).
19. M. Pahlow, D. Müller, M. Tesche, H. Eichler, G. Feingold, W. L. Eberhard, and Y.-F. Cheng, "Retrieval of aerosol prop-

erties from combined multiwavelength lidar and sunphotometer measurements," Appl. Opt. **45**, 7429–7442 (2006).
20. I. Veselovskii, A. Kolgotin, V. Griaznov, D. Müller, K. Franke, and D. N. Whiteman, "Inversion of multiwavelength Raman lidar data for retrieval of bimodal aerosol size distribution," Appl. Opt. **43**, 1180–1195 (2004).
21. D. A. Ligon, J. B. Gillespie, and P. Pellegrino, "Aerosol properties from spectral extinction and backscatter estimated by an inverse Monte Carlo method," Appl. Opt. **39**, 4402–4410 (2000).
22. J. Kaipio and E. Somersalo, *Statistical and Computational Inverse Problems* (Springer-Verlag, 2004).
23. A. Papoulis, *Probability, Random Variables, and Stochastic Processes* (McGraw-Hill, 1991).
24. D. Müller, U. Wandinger, D. Althausen, and M. Fiebig, "Comprehensive particle characterization from three-wavelength Raman-lidar observations: case study," Appl. Opt. **40**, 4863–4869 (2001).
25. B. R. Herman, B. Gross, F. Moshary, and S. Ahmed, "Methods of assessing uncertainty in determining particle size distribution parameters from optical backscatter and extinction measurements," Proc. SPIE **5154**, 208–215 (2003).
26. W. R. Gilks, S. Richardson, and D. J. Spiegelhalter, eds., *Markov Chain Monte Carlo in Practice* (Chapman & Hall, 1996).
27. J. Tamminen, "Validation of nonlinear inverse algorithms with Markov chain Monte Carlo method," J. Geophys. Res. **109**, D19303 (2004).